Journal of Molecular Structure 1199 (2020) 127011

Contents lists available at ScienceDirect

Journal of Molecular Structure

journal homepage: http://www.elsevier.com/locate/molstruc

$H_5BW_{12}O_{40}$-Catalyzed syntheses of 1,4-dihydropyridines and polyhydroquinolines *via* Hantzsch reaction: Joint experimental and computational studies

Tayebeh Momeni [a], Majid M. Heravi [a, **], Tayebeh Hosseinnejad [a], Masoud Mirzaei [b, *], Vahideh Zadsirjan [a]

[a] Department of Chemistry, Alzahra University, Vanak, Tehran, Iran
[b] Department of Chemistry, Faculty of Science, Ferdowsi University of Mashhad, Mashhad, Iran

ARTICLE INFO

Article history:
Received 27 July 2019
Received in revised form
30 August 2019
Accepted 31 August 2019
Available online 4 September 2019

Keywords:
1,4-Dihydropyridines
Keggin
Hantzsch reaction
Dimedone
1,3-Cyclohexanediones
Polyhydroquinoline
DFT

ABSTRACT

A series of polyhydroquinoline derivatives were effectively synthesized *via* Hantzsch reaction in high yields in the presence of catalytic amounts of a highly negatively charged borotungstic acid H5BW12O40 in refluxing EtOH under green and mild reaction conditions. It is a Keggin-type heteropoly acid with a higher negative charge and strong Brønsted acidity. Moreover, a comparative mechanistical analysis of Hantzsch reaction was made based on the structural, thermodynamical and electronic properties along the reaction pathway using density functional theory (DFT) and quantum theory of atoms in molecules (QTAIM) approaches.

1. Introduction

Multicomponent reactions (MCRs) have attracted much attention and stirred up the interest of synthetic organic chemists as well as those who are engaged in combinatorial chemistry due to their broad increment of molecular diversity and high atom economy effectiveness [1,2]. Although, MCRs can provide a library of interesting organic compounds and conducted in a one pot fashion, they still agonize from several drawbacks, such as usage of excessive amount of reagents and toxic solvents, some should have been performed under harsh reaction conditions and requiring long reaction time [3].

The Hantzsch pseudo-four-component reaction is the oldest (this reaction was reported by Arthur Rudolf Hantzsch in 1881) and most generally established strategy for the synthesis of 1,4-DHPs and their derivatives, several of them were found being biologically, pharmacologically and medicinally are very important compounds. As a matter of fact, nowadays, some important prescribed drug such as nifedipine A (with the brand name of Adalat) as well as amlodipine and B, nicardipine C (Fig. 1) are known as a major Ca^{2+} channels blockers, that are extensively used for treatment of several conditions such as hypertension and angina (Fig. 1) [4,5].

4-Aryl-1,4-dihydropyridines are found being analogues of NADH coenzymes, which have been known for acting as calcium channel blockers. Their unique heterocyclic moieties are found in a several bioactive compounds such as bronchodilator, antiatherosclerotic, antitumor, vasodilator, antidiabetic, geroprotective, and heptaprotective agents [6]. Due to these biological importance, polyhydroquinoline derivatives not only have stirred up the interest of organic synthetic chemists but also represent a challenging research area. Thus, several approaches have been achieved and reported for their synthesis. Among them, the most familiar and frequently operated is the classical Hantzsch MCR including, an appropriate aldehyde, ethyl acetoacetate, and ammonia as source of nitrogen in AcOH or alcohols under reflux conditions [7,8]. Nevertheless, these methods show their merits as well suffer from many

* Corresponding author.
** Corresponding author.
E-mail addresses: mmheravi@alzahra.ac.ir (M.M. Heravi), mirzaeesh@um.ac.ir (M. Mirzaei).

https://doi.org/10.1016/j.molstruc.2019.127011
0022-2860/

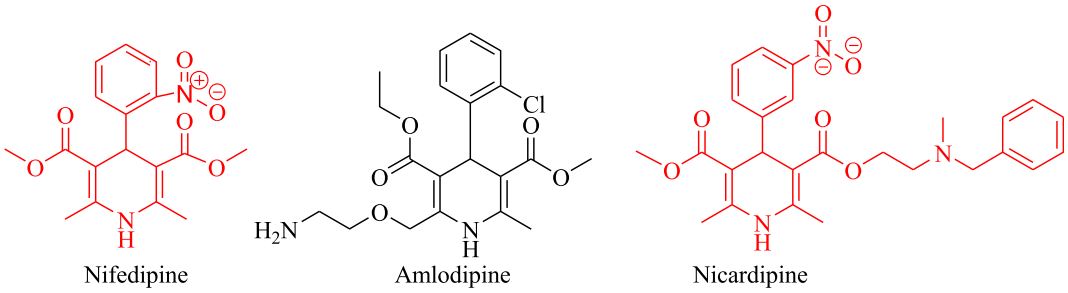

Fig. 1. Selected examples of 1,4-dihydropyridines (DHPs) demonstrating pharmacological activity.

drawbacks such as a being done in long reaction times, requiring an excess of organic solvent, giving low product yields, and under harsh refluxing conditions. Thus, introductions of other alternative methods for the synthesis of polyhydroquinoline derivatives, which are more effective, being performed under milder reaction conditions and giving higher product yields [9] are still in much demand.

Keggin type heteropoly acids (HPAs) are the most effective and promising solid acid as proton donors. HPAs are hydrous acids which retain the highest proton conductivity at ambient temperature in comparison with other inorganic solid acids as proton doners [10–14]. HPAs are placed in to a large family of metal–oxygen clusters of early transition metals with general formula of $H_z[X_xM_mO_y]$, in which M is the addenda atom and X is the heteroatom [14–16]. Two acquainted HPAs are silicotungstic acid (SiWA, $H_4SiW_{12}O_{40}$) and phosphotungstic acid (PWA, $H_3PW_{12}O_{40}$) which both have the same Keggin structure (*i.e.* x = 1, m = 12, and y = 40). A Keggin-type heteropoly acid has a higher negative charge and strong Brønsted acidity. An increase in the number of protons in Keggin heteropolyanions decreases the acidic strength [17,18].

We are interested in the catalytic activity of HPAs in organic transformations [19–21] especially those leading to construction of different heterocycles *via* MCR [23]. In this regard we have reviewed the applications of HPAs as effective catalysts, from different points of view [24,25]. In continuation of theses interests, in this paper we successfully examined a highly negatively charged borotungstic acid H5BW12O40 (hereafter denoted as BWA), where B^{3+} is the central heteroatom, as an effective catalyst in the synthesis of a series of polyhydroquinoline derivatives *via* the Hantzsch pyridine synthesis. Concentrated on joint experimental and computational methods, as the authors we have recently reviewed the synthesis and properties of Hantzsch-type compounds *via* combined experimental and computational viewpoints [26].

In continuation of our recent interest in joint experimental and computational investigations on the synthesis and design of heterogeneous catalysts [27–30] and also mechanistical properties of catalyzed organic reactions [31–33], In this respect, we applied quantum chemistry approaches to obtain accurate computational information on the energetics and electronic aspects of reaction pathways and present sound interpretations on the priority of its mechanistically aspects and feature.

2. Experimental

All chemicals employed to study of the catalytic behavior of the BWA were purchased from Aldrich Merck Company and used as received without further purification. Heteropoly acid, $H_5BW_{12}O_{40}$ (BWA) was prepared, following the literature [34]. Melting points were measured by an electrothermal 9200 apparatus. IR spectra were recorded on the FT-IR Tensor Spectrophotometer. Nuclear magnetic resonance (NMR) spectra were recorded on a Bruker AVANCE 400 MHz Spectrometer in $CDCl_3$ as a solvent. All products were known, thus the synthesis of the products were conventionally confirmed by comparison of their melting points, measured by using the capillary tube method with an electro thermal 9200 apparatus, and FTIR spectra with authentic samples. As a matter of certainty, the ^{1}H NMR spectra of compounds **5c** and **5f** were measured and the for some selected products, NMR spectra are also given with the related references.

2.1. Synthesis of 1,4-dihydropyridines and 4-Aryl-1,4-dihydropyridines: General Procedure.

A mixture of an appropriate aldehyde (1 mmol), ammonium acetate (1 mmol) and ethylacetoacetate (2 mmol) or dimedone (1 mmol), ethylacetoacetate (1 mmol) in the presence of catalytic amount of ($H_5BW_{12}O_{40}$) (10 mol %) was refluxed in EtOH (5 ml) for the indicated reaction time. The progress of the reaction was monitored by TLC (7:3 n-hexane/ethylacetate). After the completion of the reaction, water (5 ml) was added to the mixture. The organic layer was extracted with ethyl acetate, dried over anhydrous sodium sulphate and filtered using an ordinary funnel and filter paper by gravity. The filtrate was evaporated under reduced pressure and the crude products were purified by recrystallization from a mixture of ethylacetate/*n*-hexane to give the corresponding products. These products were identified by comparison of their melting points along with their FTIR spectra and in two cases (**5c** and **5f**) ^{1}H NMR.

2.2. Selected spectral data

2.2.1. Ethyl-2,7,7-trimethyl-5-oxo-4-phenyl-1,4,5,6,7,8-hexahydroquinoline- 3-carboxylate (5a):[35]

FT-IR (KBr): υ_{max} = 3288, 3218, 3080, 3029, 2959, 2930, 1871, 1699, 1610, 1484 cm^{-1}; ^{1}H NMR ($CDCl_3$, 300 MHz): δ = 0.92 (3H, s, $-CH_3$), 1.04 (3H, s, $-CH_3$), 1.21 (3H, t, *J* = 7.20 Hz, $-CH_3$), 2.10–2.26 (4H, m, $-CH_2$), 2.30 (3H, s, $-CH_3$), 4.06 (2H, q, *J* = 7.20 Hz, $-OCH_2$), 4.66 (1H, s, –CH) 5.05 (NH, s), 7.11–7.31 (5H, m, Ar–H). ^{13}C NMR ($CDCl_3$, 75 MHz): δ = 14.42, 19.55, 27.33, 29.77, 32.93, 36.88, 41.02, 51.04, 60.03, 106.17, 112.13, 126.22, 128.18, 128.23, 144.08, 147.33, 149.26, 167.73, 196.09.

2.1.2. Ethyl-2,7,7-trimethyl-5-oxo-4-p-tolyl-1,4,5,6,7,8-hexahydroquinoline-3-carboxylate (5b) [35]

FT-IR (KBr): υ_{max} = 3275, 3206, 3022, 2930, 1702, 1647, 1492 cm^{-1}; ^{1}H NMR ($CDCl_3$, 300 MHz): δ = 0.94 (3H, s, $-CH_3$), 1.06 (3H, s, $-CH_3$), 1.22 (3H, t, *J* = 6.40 Hz, $-CH_3$), 2.11–2.21 (4H, m, $-CH_2$), 2.25 (3H, s, $-CH_3$), 2.33 (3H, s, $-CH_3$), 4.07 (2H, q, *J* = 6.40 Hz, $-OCH_2$), 5.00 (1H, s, –CH), 6.49 (NH, s), 7.00 (2H, d, *J* = 7.60 Hz, Ar–H), 7.19 (2H, d, *J* = 8.0 Hz Ar–H). ^{13}C NMR ($CDCl_3$, 75 MHz): δ = 14.51, 19.52, 21.36, 27.43, 29.79, 32.93, 36.39, 41.14, 51.09, 60.04, 106.36, 112.39, 128.13, 128.80, 135.63, 143.82, 144.51, 148.94, 167.87, 195.92.

2.2.3. Ethyl-2,7,7-Trimethyl-5-oxo-4-(4-methoxyphenyl)-1,4,5,6,7,8 hexahydroquinoline −3 -carboxylate (5c) [36]

FT-IR (KBr): υ_{max} = 3276, 2957, 1701, 1648, 1605, 1494, 1380, 1215, 1033 cm^{-1}; ^1H NMR($CDCl_3$, 300 MHz) δ = 0.94 (3H, s, $-CH_3$), 1.07 (3H, s, $-CH_3$), 1.21 (3H, t, *J* = 7.2 Hz, $-CH_3$), 2.13−2.27 (3H, m, $-CH_2$), 2.31−2.37 (4H, m, $2CH_2$), 3.74 (3H, s, $-CH_3$), 4.06 (2H,q, *J* = 7.2 Hz, OCH_2), 5.00 (1H, s, CH), 6.01 (1H, s, NH), 6.72−6.75 (2H, m, Ar−H), 7.20−7.26 (2H, m, Ar−H). ^{13}C NMR ($CDCl_3$, 75 MHz): δ = 14.2, 16.3, 27.2, 27.2, 31.7, 41.7, 43.5, 51.3, 55.9, 61.7, 102.3, 111.9, 114.2, 130.1, 134.5, 149.5, 150.7, 157.7, 167.2, 198.9.

2.2.4. Ethyl-2,7,7-trimethyl-4-(3-nitrophenyl)-5-oxo-1,4,5,6,7,8hexahydroquinoline-3-carboxylate (5d) [35]

FT-IR (KBr): υ_{max} = 3283, 3210, 3076, 2957, 1704, 1643, 1534, 1485, 1380, 1351, 1210 cm^{-1}; ^1H NMR (400 MHz, $CDCl_3$) δ = 8.11 (1H, t, *J* = 1.8 Hz, Ar−H), 8.02−7.94 (1H, m, Ar−H), 7.73 (1H, d, *J* = 7.7 Hz), 7.37 (1H, t, *J* = 7.9 Hz), 6.39 (1H, d, *J* = 6.6 Hz, −NH), 5.16 (1H, s, −CH), 4.07 (2H, q, *J* = 7.1 Hz, $-OCH_2$), 2.42−2.11 (7H, m), 1.20 (3H, t, *J* = 7.1 Hz, $-CH_3$), 1.09 (3H, s, $-CH_3$), 0.93 (3H, s, $-CH_3$). ^{13}C NMR ($CDCl_3$, 75 MHz): δ = 19.5; 27.0; 29.3; 32.7; 36.7; 40.9; 50.5; 51.2; 104.8; 111.2; 121.3; 122.6; 128.7; 134.7; 144.7; 148.3; 164.7; 167.3; 195.5.

2.2.5. Ethyl-2,7,7-trimethyl-4-(4-nitrophenyl)-5-oxo-1,4,5,6,7,8 hexahydroquinoline - 3-carboxylate (5e) [35]

FT-IR (KBr): υ_{max} = 3275, 3190, 3073, 2965, 1703, 1648, 1517, 1492, 1376, 1344, 1279 cm^{-1}; ^1H NMR ($CDCl_3$, 300 MHz):δ = 0.90 (3H, s, $-CH_3$), 1.08 (3H, s, $-CH_3$), 1.82 (3H, t, *J* = 7.10 Hz, $-CH_3$), 2.16−2.36 (4H, m, $-CH_2$), 2.40 (3H, s, $-CH_3$), 4.04 (2H, q, *J* = 7.80 Hz, $-OCH_2$), 5.15 (1H, s, −CH), 6.31 (NH, s), 7.50 (2H, d, *J* = 7.80 Hz, Ar−H), 8.09 (2H, d, *J* = 7.8 Hz, Ar−H). ^{13}C NMR ($CDCl_3$,75 MHz): δ = 14.33, 18.97, 27.03, 29.57, 32.54, 37.29, 50.74, 59.79,103.47, 110.27, 123.14, 129.03, 145.99, 146.04, 150.294, 155.23,167.14, 195.47.

2.2.6. Ethyl 4-(4-chlorophenyl)-2,7,7-trimethyl-5-oxo-1,4,5,6,7,8-hexahydroquinoline-3-carboxylate (5f). [37]

FT-IR (KBr): υ_{max} = 3274, 3206, 3076, 2934, 2871, 1706, 1604, 1491, 1381, 1214, 1108, 856. cm^{-1}; ^1H NMR (DMSO, 400 MHz): δ = 0.84 (s, 3H, $-CH_3$), 0.99 (s, 3H, $-CH_3$), 1.14 (t, 3H, *J* = 7.2 Hz, $-CH_3$), 2.06 (dd, 2H, $-CH_2$), 2.13 (dd, 2H, $-CH_2$), 2.28 (s, 3H, $-CH_3$), 3.99 (q, 2H, *J* = 7.3 Hz, $-OCH_2$), 4.95 (s, 1H, −CH), 7.08 (d, 2H, *J* = 9.3 Hz, Ar−H), 7.18 (d, 2H, *J* = 9.4 Hz, Ar−H), 7.93 (1H, −NH−). ^{13}C NMR (DMSO, 100 MHz): δ = 14.8, 19.2, 27.4, 29.9, 32.8, 36.6, 40.8, 51.2, 60.1, 77.8, 105.3, 111.5, 128.2, 129.8, 131.7, 146.5, 150.1, 167.8, 195.7;

2.2.7. Ethyl-4-(4-bromophenyl)-2,7,7-trimethyl-5-oxo-1,4,5,6,7,8-hexahydroquinoline-3-carboxylate (5g) [35]

FT-IR (KBr): υ_{max} = 3275, 3242, 3075, 2959, 2935, 1703, 1648, 1604, 1421, 1380, 1279, 1214, 1071, 842, 533. cm^{-1}; ^1H NMR ($CDCl_3$, 300 MHz): δ = 0.91 (3H, s, $-CH_3$), 1.06 (3H, s, $-CH_3$), 1.19 (3H, t, *J* = 7.10 Hz,$-CH_3$), 2.14−2.32 (4H, m, $-CH_2$), 2.35 (3H, s, $-CH_3$), 4.05 (2H, q, *J* = 7.10 Hz, $-OCH_2$), 5.00 (1H, s, −CH), 6.58 (NH, s), 7.19 (2H, d, *J* = 7.60 Hz, Ar−H), 7.30 (2H, d, *J* = 7.70 Hz, Ar−H). ^{13}CNMR ($CDCl_3$, 75 MHz): δ = 14.44, 19.63, 27.35, 29.74, 32.98, 36.54, 41.18, 50.98, 60.14, 105.89, 111.84, 120.09, 130.04, 131.10, 144.14, 146.46, 149.06, 167.54, 195.98.

2.2.8. Diethyl-2,6-dimethyl-4-phenyl-1,4-dihydropyridine-3,5-dicarboxylate (6a) [35]

FT-IR (KBr): υ_{max} = 3342, 2934, 1689, 1651, 1489, 1247, 1123, 1090, 701 cm^{-1}; ^1H NMR ($CDCl_3$, 300 MHz): δ = 1.22 (6H, t, *J* = 7.05 Hz, $-CH_3$), 2.31 (6H, s, $-CH_3$), 4.09 (4H, q, *J* = 6.80 Hz, $-OCH_2$), 4.99 (1H, s, −CH), 5.81 (NH, s), 7.14−7.25 (5H, m, Ar−H). ^{13}C NMR ($CDCl_3$, 75 MHz): δ = 14.52, 19.81, 39.84, 60.02, 104.12, 126.31, 128.06, 128.21, 144.45, 148.02, 168.09.

2.2.9. Diethyl 2,6-dimethyl-4-(4-methoxyphenyl)-1,4-dihydropyridine-3,5-dicarboxylate (6b) [38]

FT-IR (KBr): υ_{max} = 3233, 2933, 2804, 1656, 1609, 1489, 1515, 1251, 1198, 1041, 568 cm^{-1}, ^1H NMR: (DMSO, 300 MHz): δ = 8.73 (s, 1H, NH), 7.03 (d, 2H, *J* = 8.4 Hz, Ar−H), 6.74 (d, 2H, *J* = 8.4 Hz, Ar−H), 4.78 (s, 1H), 397 (m, 4H, $2CH_2$), 3.66 (s, 3H, $-OCH_3$), 2.23 (s, 6H, $2CH_3$), 1.12 (t, 6H, *J* = 7.2 Hz, $2CH_3$); ^{13}C NMR (DMSO, 100 MHz): δ = 166.9, 157.4, 144.9, 140.4, 128.2, 113.1, 102.1, 58.9, 54.8, 37.9, 18.1, 14.1.

2.2.10. Diethyl2,6-dimethyl-4-(3-nitrophenyl)-1,4-dihydropyridine-3,5-dicarboxylate (6c) [38]

FT-IR (KBr): υ_{max} = 3345, 2988, 1707, 1645, 1528, 1486, 1352, 1214, 1044, 788 cm^{-1};^1H NMR: (DMSO, 300 MHz): δ = 8.99 (s, 1H, NH), 7.98 (dd, 1H, *J* = 2.1 Hz, Ar−H), 7.55 (m, 3H), 4.94 (s, 1H), 3.97 (m, 4H, $2CH_2$), 2.27 (s, 6H, $2CH_3$), 1.10 (t, 6H, *J* = 7.2 Hz, $2CH_3$); ^{13}C NMR (DMSO, 75 MHz): δ = 166.4, 150.2, 147.3, 146.3, 134.1, 129.5, 121.8, 121.0, 101.0, 59.1, 39.2, 18.1, 14.0.

2.2.11. Diethyl 2,6-dimethyl-4-(4-nitrophenyl)-1,4-dihydro pyridine-3,5-dicarboxylate (6d) [39]

FT-IR (KBr): υ_{max} = 3248, 3102, 1647, 1518, 1488, 1347, 1252, 863. cm^{-1}; ^1H NMR (DMSO, 400 MHz): δ = 1.27 (t, 6H, *J* = 7.3 Hz, $-CH_3$), 2.13 (s, 6H, $-CH_3$), 4.35 (m, 4H, *J* = 5.9 Hz, $-OCH_2$), 4.85 (1H, −NH−), 5.79 (s, 1H, −CH), 7.51 (d, 2H, *J* = 7.8 Hz, Ar−H), 7.59 (d, 2H, *J* = 7.8 Hz, Ar−H); ^{13}C NMR (DMSO, 100 MHz): δ = 15.1, 17.8, 45.7, 63.3, 96.6, 128.1, 128.7, 132.5, 145.2, 148.3, 167.5.

2.2.12. Diethyl 4-(4-bromophenyl)-2,6-dimethyl-1,4-dihydro-pyridine-3,5-dicarboxylate (6e) [40]

FT-IR (KBr): υ_{max} = 3345, 1707, 1645, 1486, 1214, 1044, 788 cm $^{-1}$; ^1H NMR ($CDCl_3$, 250 MHz): δ = 1.25 (t, 6H, *J* = 7.1 Hz, $2CH_3CH_2$), 2.29 (s, 6H, $2CH_3$), 4.10 (q, 4H, *J* = 7.1 Hz, $2CH_3CH_2$), 4.96 (s, 1H, CH), 6.47 (s, 1H, NH), 7.16 (d, 2H, *J* = 8.4 Hz, Ar−H), 7.33 (d, 2H, *J* = 8.4 Hz, Ar−H); ^{13}C NMR ($CDCl_3$, 62.9 MHz): δ = 14.2, 19.3, 39.3, 59.8, 103.4, 119.8, 130.0, 130.8, 144.5, 146.9, 167.6.

2.2.13. Diethyl 4-(4-chlorophenyl)-2,6-dimethyl-1,4-dihydropyridine-3,5-dicarboxylate (6f) [39]

FT-IR (KBr): υ_{max} = 3357, 2987, 1694, 1486, 1461, 1333, 1261, 881 cm^{-1}; ^1H NMR (DMSO, 400 MHz): δ = 1.23 (t, 6H, *J* = 7.1 Hz, $-CH_3$), 2.27 (s, 6H, $-CH_3$), 4.17 (m, 4H, *J* = 5.7 Hz, $-OCH_2$), 4.87 (1H, −NH−), 5.68 (s, 1H, −CH), 7.41 (d, 2H, *J* = 7.9 Hz, Ar−H), 7.57 (d, 2H, *J* = 7.8 Hz, Ar−H); ^{13}C NMR (DMSO, 100 MHz): δ = 14.3, 14.9, 45.9, 61.3, 97.6, 127.1, 128.3, 134.8, 143.2, 147.1, 167.

3. Results and discussion

We recently reviewed the applications of dimedone in the synthesis of various hetrocyclic systems including the synthesis of polyhydroquinoline *via* Hantzsch reaction [41]. During our last longing experiences (about 2 decades) a specific HPA so-called $H_5BW_{12}O_{40}$ (BWA), has attracted our special attention. Since this heteropoly acid has B^{3+} as the central heteroatom, we thought it is worthy to test its catalytic activity as an easily accessible (inexpensively) catalyst and compare it with that of known but expensive and not easily to handle boron tetrafluoride etherate [42−44] as a strong Lewis acid in the synthesis of different heterocycles *via* MCR which has been our ever interest for the years.

To obtain the polyhydroquinoline derivatives *via* Hantzsch reaction, different Lewis acids such as $TiCl_2$/Nano-γ-Al_2O_3 [45], [$Ce(SO_4)_2 \cdot 4H_2O$] [46], Zr-SBA-16 [47], and Brønsted acids such [$(CH_2)_4SO_3HMIM$][HSO_4] [48], MIL-101-SO_3H [49], ([DDPA][HSO_4])

[50] have been used as effective catalysts.

Armed with these experiences, initially, in the presence of BWA as an acidic catalyst, in ethanol as solvent, at reflux condition, a four-component reaction (as a model reaction) involving, benzaldehyde, ethylacetoacetate, dimedone, and ammonium acetate was performed. The progress of reaction was monitored by TLC (using 7:3 n-hexane/ethylacetate as eluent). This reaction was proceeded smoothly and cleanly, to completion to give the corresponding polyhydroquinoline derivative in satisfactory yield (Scheme 1).

The reaction conditions were optimized using the aforementioned model reaction comprising benzaldehyde, ethylacetoacetate, dimedone, and ammonium acetate. The results are shown in Table 1. We performed the model reaction by grinding, under solvent-free conditions, the reaction proceeded, insignificantly. Then, we added our catalyst to the above system. By grinding the mixture, the reaction proceeded, sluggishly. Thus, we then examined the effects of solvents, both, polar and nonpolar. To select the best solvent, the model reaction was run in refluxing water as the green and plentiful solvent which gave the desired compound **5a** in 27% yield (Table 1, entry 1).

In addition to water, we examined, EtOH/H_2O, CH_2Cl_2, CH_3CN, $CH_3COOCH_2CH_3$. As indicated in Table 1, when the model reaction was run in EtOH/H_2O at reflux temperature, gave the expected product **5a** in only 63% yield (Table 1, entry 3). When CH_2Cl_2 was used product 5a was obtained in 20% yield (Table 1, entry 2). $CH_3COOCH_2CH_3$ and CH_3CN gave the respective products in, 13 and 57% yield respectively (Table 1, entries 4 and 5) and in solvent-free conditions provided the corresponding products in 72% yield (Table 1, entries 6). Particularly, the best results (94% yields) was obtained when the model reaction was conducted in EtOH at reflux temperature (Table 1, entry 7). Thus, EtOH was selected as the solvent of choice. In order to find the influence of temperature, the model reaction was conducted in the presence of $H_5BW_{12}O_{40}$ (BWA) in EtOH at ambient temperature giving only 50% yield (Table 1, entry 8). This model reaction then was refluxed in EtOH which resulted in the desired products in highest yield (94% yield) (Table 1, entry 6). At last, to optimize the catalyst loading we conducted the model reaction in the presence of 5 mol%, BWA. The expected product was isolated at 85%, showing the importance of the presence of a catalyst particularly a one such as BWA, (Table 1, entry 9). Then, traditionally, we increased the amount gradually from 5 mol% to 10 mol%. The yield of reactions was increased from 85% to 94% (Table 1, entry 7). The improvement of the yield by increasing the BWA quantity can be rationalized to the possible increase in the number of available active sites, as well as increasing the amount of contact and collision chance between the BWA surface with the molecules of the starting materials. Notably, that further increase in the loaded BWA amount from 10 mol% to 15 mol % the yields and reaction times did not change, significantly. (Table 1, entry 10). Thus, 10 mol% of catalyst selected as the optimal catalyst loading (Table 1, entry 7). The best results were obtained when 1 mmol of aldehyde, 1 mmol of dimedone, 1 mmol of ammonium acetate and 10 mol% $H_5BW_{12}O_{40}$ (BWA) in EtOH was refluxed to give the corresponding desired product in 94% yield

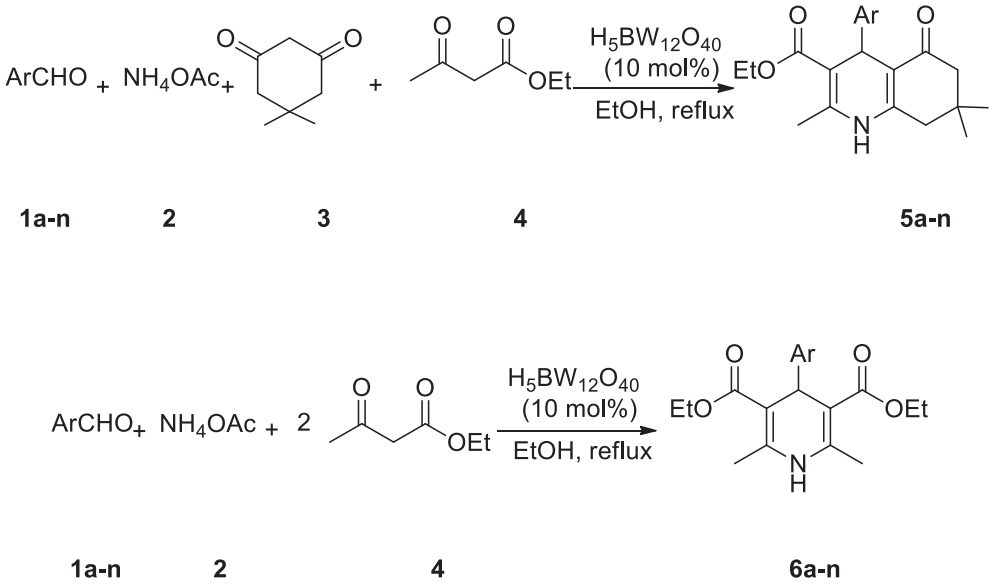

Scheme 1. $H_5BW_{12}O_{40}$ catalyzed symmetrical and unsymmetrical Hantzsch reaction.

Table 1
Optimization of reaction conditions for Hantzsch reaction.

Entry	Solvent	Temperature	Time (min)	Catalyst amount (mol%)	Yield (%)
1	H_2O	Reflux	600	10	27
2	CH_2Cl_2	Reflux	720	10	20
3	EtOH/H_2O	Reflux	240	10	63
4	CH_3COOEt	Reflux	420	10	13
5	CH_3CN	Reflux	120	10	57
6	Non-solvent	Reflux	120	10	72
7	EtOH	Reflux	45	10	94
8	EtOH	Room	120	10	50
9	EtOH	Reflux	60	5	85
10	EtOH	Reflux	45	15	94

Table 2
$H_5BW_{12}O_{40}$ catalyzed Hantzsch reaction under reflux condition in EtOH.

Entry	Product	R^1	Yield (%)	Time (min)	mp (°C) Found	mp (°C) Lit
1	5a	H	94	45	195–199	202-204 [36]
2	5b	4-CH_3	91	60	255–257	259-261 [36]
3	5c	4- OCH_3	92	60	255–257	255-257 [35]
4	5d	3-NO_2	93	50	180–183	173-177 [36]
5	5e	4-NO_2	98	45	235–240	241-243 [36]
6	5f	4-Cl	90	45	240–242	244-246 [35]
7	5g	4-Br	90	45	253–255	254-256 [38]
8	5h	2-OCH_3	88	60	238–240	–
9	6a	H	87	90	135–140	140-142 [40]
10	6b	4-OCH_3	85	100	160–161	163-168 [40]
11	6c	3-NO_2	88	90	158–160	163-164 [40]
12	6d	4-NO_2	89	90	124–127	128-132 [40]
13	6e	4-Br	84	90	160–164	162-164 [39]
14	6f	4-Cl	84	90	140–143	145-147 [40]

after 45 min (Table 1, entery 7).

Under the optimal conditions, we investigated the substrate scopes and limitations of this MCR Various aromatic aldehydes containing both electron-releasing or electron-withdrawing substituents on the aromatic ring in the ortho, meta, and para positions, gave the corresponding products in high yields as indicated in Table 2.

To compare the advantages of this catalyst, its catalytic activity was compared by those other catalyst, previously reported, such as silica coated nano-Fe_3O_4 supported basic ionic liquid (BIL@MNP) [36], γ-Al_2O_3-nanoparticles [42], molecular sieve supported lanthanum [43], Bakers' yeast [47], Ionic liquid (TBA-AMPS) [44] (Table 3). As can be seen in Table 3, the catalytic activity of BWA was compared with diverse catalysts such as which have been previously employed as catalysts in our model reaction. As it can compared BWA is doing best among others, catalyst can mediate. In addition, it provides the corresponding products in short reaction time.

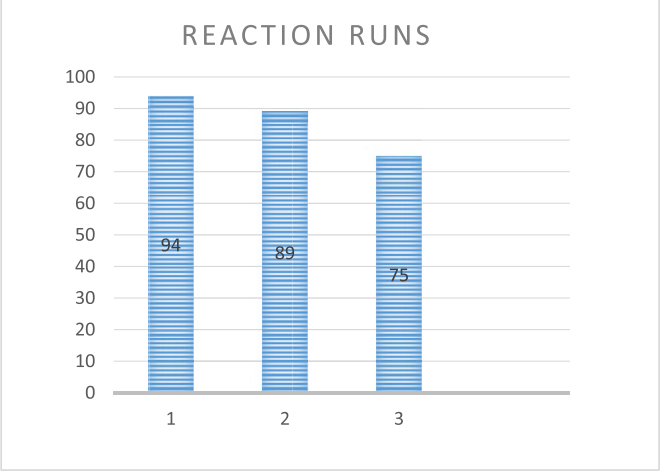

Fig. 2. Recyclability of catalyst for Hantzsch reaction.

3.1. Catalyst reusability

Noticeably, as it can be realized from Fig. 2, we studied the reusability of the catalyst. Initially, the model reaction was done in the presence of the freshly prepared BAW under the already secured optimal reaction. The catalyst was soluble in EtOH and could be removed easily by evaporation of the solvent. After recovery of the catalyst, it was washed with EtOAc, dried at 130 °C for 1 h, and re-used in the same model reaction. The recycled catalyst and recycled catalyst were used for three consecutive reactions

Table 3
The comparison of the catalytic activity of $H_5BW_{12}O_{40}$ with formerly reported catalysts.

Entry	Catalyst	Time	Catalyst Amount	Temperature	Solvent	Yield (%)	Ref.
1	silica coated nano-Fe_3O_4 supported basic ionic liquid (BIL@MNP)	15 min	0.25 mmol%	70 °C	Solvent free	92	[36]
2	γ-Al_2O_3-nanoparticles	10 min	0.2 mg	90 °C	Solvent free	92	[42]
3	Ionic liquid (TBA-AMPS)	8 min	10 mmol%	reflux	CH_3OH	97	[43]
4	Molecular sieve supported lanthanum	4 h	10 mg	reflux	EtOH	99	[44]
5	Tetrabutylammonium hexatungstate $[TBA]_2[W_6O_{19}]$	20 min	7 mmol%	110 °C	Solvent free	95	[51]
6	$K_7[PW_{11}CoO_{40}]$	25 min	10 mmol%	reflux	CH_3CN	85	[45]
7	Bakers' yeast	24 h	200 mg	r.t.	phosphate buffer	79	[46]
8	LiBr	4 h	10 mol%	r.t.	EtOH	93	[47]
9	Ceric Ammonium Nitrate (CAN)	60 min	0.05 mmol%	r.t.	EtOH	92	[10]
10	Hafnium (IV) bis(perfluorooctanesulfonyl)imide $Hf(NPf_2)_4$	3 h	1 mol%	60 °C	perfluorodecalin	95	[35]
11	I_2	90 min	30 mol%	25 °C	EtOH	93	[48]
12	ZnO-nanoparticle	20 min	10 mol%	r.t.	Solvent-free	98	[49]
13	Alumina sulfuric acid (ASA)	120 min	0.2 g	70 °C	MeOH	92	[41]
14	Ni nanoparticle	1 min	10 mol%	microwave (540 W)	Neat	95	[50]
15	nickel containing alkyl-imidazolium ionic liquid based ordered mesoporous organosilica (Ni@ILOMO)	15 min	0.5 mol%	70 °C	Solvent-free	96	[52]
16	PdRuNi nanoparticles furnished with graphene oxide (PdRuNi@GO NPs)	45 min	6 mg	70 °C	DMF	93	[53]
17	(SnO_2) nanoparticles	9 min	1 mol%	r.t.	EtOH	94	[37]
18	Mesoporous vanadium ion doped titania nanoparticles (V–TiO_2)	10 min	2 mol%	r.t.	Solvent-free	85	[54]
19	$Yb(OTf)_3$	5 h	5 mol%	r.t.	EtOH	90	[55]
20	$H_5BW_{12}O_{40}$	45 min	10 mol%	reflux	EtOH	94	This work

without appreciable loss in its catalytic activities.

4. Computational section

In the present section, we have concentrated to assess computationally two mechanistical pathways of Hantzsch reaction that lead to produce 1,4-dihydropyridine and 2-arylpyridine as has been reported experimentally [56]. In this respect, we have presented accurate computational information on the energetics of these two reaction pathways using quantum chemistry methods. It should be mentioned that in our previous researches, we have mechanistically studied the origins of regio-selectivity in the sonogashira and click synthesis of triazoles and tetrazoles [31–33] *via* density functional theory (DFT) computations.

In this line, we first designed two different reaction pathway models to investigate the reaction energetics that led to generate two different products entitled as product-1 and product-2, respectively, as was illustrated in Scheme 2.

All calculations were performed using GAMESS suite of programs [57] *via* DFT approach, based on M08-HX functional in

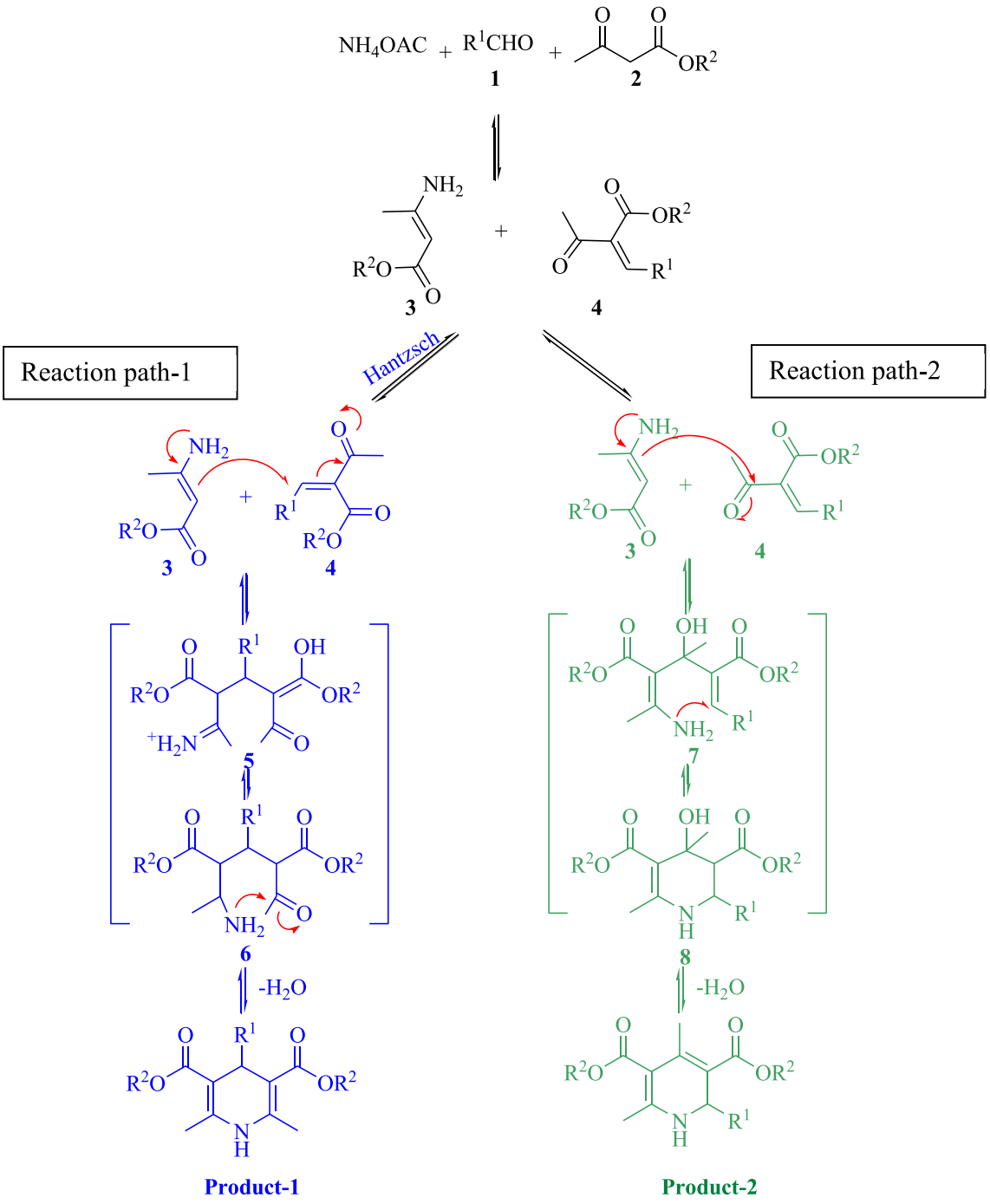

Scheme 2. Plausible mechanisms for the synthesis of 1,4-dihydropyridine and 2-arylpyridines *via* two reaction paths.

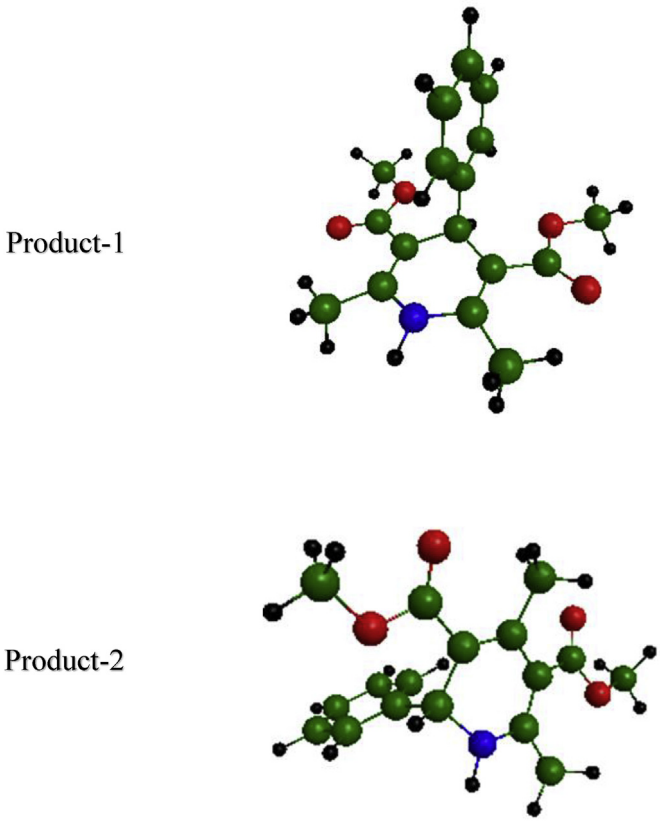

Fig. 3. The optimized structure of product-1 and product-2, calculated at M08-HX/6-311 + G** level of theory.

connection with 6-311 + G** orbital basis sets [58]. We have determined the ground state structures of all reagents and products through the geometry optimization procedure. The harmonic frequency analysis was then performed to confirm that the found optimized geometries correspond to the true minima and also to obtain enthalpies and Gibbs free energies. Furthermore, the effect of solvation on the reaction thermochemistry in the presence of Dimethyl sulfoxide (DMSO) and ethanol (EtOH) was taken into account using the polarized continuum model (PCM) computations. In Fig. 3, we have displayed the optimized structure of product-1 and product-2, calculated at M08-HX/6-311 + G** level of theory. The calculated thermochemical data, including reaction energies, Enthalpies and Gibbs free energies at M08-HX/6-311 + G** in the gas and two solution phases are presented in Tables 4 and 5, respectively.

The comparative survey in the reported results of Tables 4 and 5 revealed that the production of product-1 in the gas and solution phases should be more favorable thermodynamically than product-2 about 7−8 kcal mol^{-1}. Expectedly, at both reaction pathways, thermochemistry in the solution phase is more stable than the gas phase with the corresponded more negative calculated Gibbs free energy values and also both solvents, DMSO and EtOH have a near and similar effect on the reaction thermochemical properties. Moreover, the calculated Gibbs free energy values become more positive than those obtained for enthalpy calculated values that could be assigned to the negative values of the reaction entropy change.

In order to explain the formation of the different products, 1,4-DHPs and 2-arylpyridines, two mechanistical pathways are suggested in Scheme 2. The initial step is the same in two reaction paths. At this stage, the reaction involves a Knoevenagel

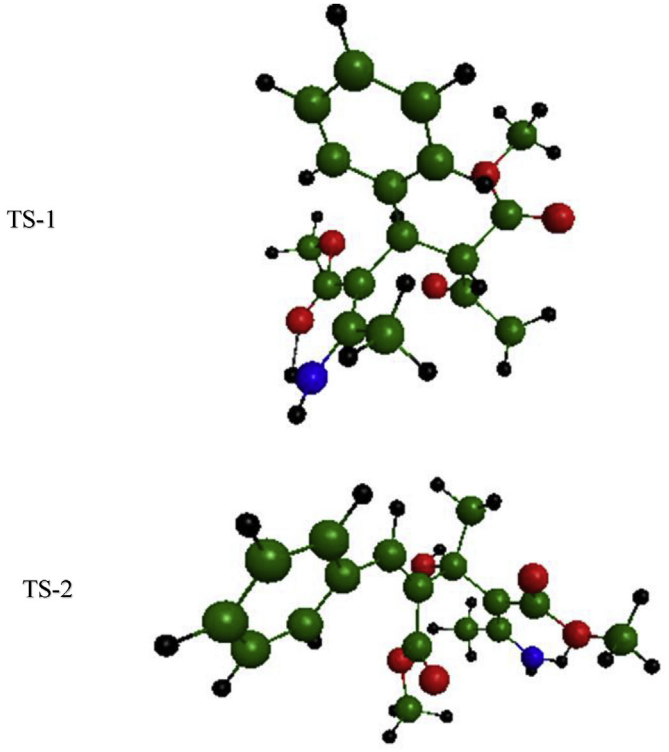

Fig. 4. Optimized structures of TS-1 and TS-2, calculated at M08-HX/6-311 + G** level of theory.

Table 4
Thermochemistry of two reaction pathways, calculated at M08-HX/6-311 + G** level of theory in the gas phase. ΔEe is the reaction energy, ΔH and ΔG are the reaction enthalpy and Gibbs free energy, respectively. Note that the conversion energy change values are in kcal.mol^{-1}.

M08-HX/6-311 + G**			
Isomers	Gas phase		
	ΔE_e	ΔH	ΔG
Product-1	−1.67	−4.15	2.38
Product-2	5.88	3.56	10.28

Table 5
The same as Table 4, calculated in the presence of DMSO and ethanol as solvents *via* PCM method.

M08-HX/6-311 + G**						
Isomers	DMSO solvent			Ethanol solvent		
	ΔE_e	ΔH	ΔG	ΔE_e	ΔH	ΔG
Product-1	−5.33	−7.74	−1.27	−5.26	−7.74	−1.20
Product-2	1.58	−0.74	5.98	1.66	−0.66	6.06

Table 6
The Gibbs free energy differences between two transition states (denoted as ΔG_{TS}) corresponded to two reaction pathways, calculated at M08-HX/6-311 + G** level of theory in the gas and two solution phases, DMSO and ethanol.

M08-HX/6-311 + G**			
	Gas phase	DMSO solvent	Ethanol solvent
ΔG_{TS} (kcal.mol^{-1})	28.44	25.34	25.42

Table 7
Mathematical properties of BCPs associated to some selected bonds in product-1 and product-2. The properties have been obtained *via* QTAIM analysis on the M08-HX/6-311 + G** calculated wave function of electron density. Note that numbering of atoms is in accordance with Fig. 5.

Product-1						
Bonded atoms	ρ_b	$\nabla^2\rho_b$	G_b	V_b	H_b	$\lvert V_b\rvert/G_b$
C_{11}–C_{13}	0.241	−0.543	0.057	−0.251	−0.193	4.342
C_{11}–C_{12}	0.241	−0.542	0.058	−0.251	−0.193	4.339
N_{16}–C_{15}	0.295	−0.686	0.239	−0.650	−0.411	2.715
C_{14}–N_{16}	0.294	−0.685	0.238	−0.649	−0.410	2.717
Product-2						
C_6–C_7	0.267	−0.658	0.072	−0.308	−0.231	4.245
C_7–C_8	0.323	−0.907	0.121	−0.470	−0.348	3.863
N_{21}–C_5	0.320	−0.712	0.290	−0.759	−0.468	2.613
C_9–N_{21}	0.252	−0.615	0.153	−0.460	−0.306	3.005

Table 8
The same as Table 5 for TS-1 and TS-2. Note that numbering of atoms is in accordance with Fig. 6.

TS-1						
Bonded atoms	ρ_b	$\nabla^2\rho_b$	G_b	V_b	H_b	$\lvert V_b\rvert/G_b$
N_{26}–C_3	0.318	−0.777	0.264	−0.722	−0.458	2.732
C_6–C_8	0.232	−0.491	0.055	−0.233	−0.178	4.210
C_8–C_{11}	0.238	−0.535	0.054	−0.242	−0.187	4.478
C_8–C_9	0.231	−0.491	0.055	−0.232	−0.177	4.235
TS-2						
N_3–C_7	0.313	−0.785	0.249	−0.694	−0.445	2.788
C_6–C_9	0.233	−0.508	0.050	−0.228	−0.177	4.497
C_4–C_9	0.241	−0.549	0.054	−0.247	−0.192	4.504
C_{20}–C_{11}	0.345	−1.026	0.145	−0.547	−0.402	3.761

condensation of 1,3-dicarbonyl compound with the aldehyde to give an α,β-unsaturated carbonyl compound 4 and a condensation of ammonia with another equivalent of the 1,3-dicarbonyl compound to afford an enamine 3. The rate determining step is the Michael addition of the enamine to the α,β-unsaturated carbonyl compound. However, unlike the previously known mechanism of the Hantzsch reaction, the enamine intermediate can attack on the carbon atom of the C═O double bond (carbon β of 4) instead of the carbon atom of the C═C double bond (carbon α of 4). Subsequently, the intermediate 7 undergoes an intramolecular addition of the amino to the carbon-carbon double bond to afford the 1,2-dihydropyridine.

In this mechanistical context, we studied comparatively the thermochemical properties of transition states species in two above-mentioned mechanistic reaction pathways *via* saddle point computations. In Fig. 4, the obtained M08-HX/6-311 + G** optimized structures of transition states, corresponded to two reaction routes have been represented (denoted as TS-1 and TS-2, respectively). In Table 6, we have listed the difference of Gibbs free energy values for TS-1 and TS-2, calculated at M08-HX/6-311 + G** levels in the gas and two solution phases, respectively. As it can be deduced from the calculated results of Table 6, TS-1 is more stable than TS-2 by around 27 kcal mol^{-1} that strictly approves the mechanistical priority in the synthesis of product-1, compared with product-2. In another hand, it was also demonstrated that the calculated stability difference between two transition state structures decreases in the solution phases in comparison with the gas phase.

In the next step, we concentrated on topological analysis of electron density functions *via* QTAIM calculations to investigate the mechanistical features of two reaction paths [59–61].

All topological analysis of electron density was performed at DFT optimized structures of products and transition states along the reaction pathways *via* QTAIM computations using AIM2000 program[57].

In this respect, resulting M08-HX/6-311 + G** wave function files for the optimized structures of products and transition states were applied as inputs to AIM2000 program. In Tables 7 and 8, we have reported the calculated values of electron density, ρb, its Laplacian, ∇2ρ, electronic kinetic energy density, Gb, electronic potential energy density, Vb, total electronic energy density, Hb and ratio of |Vb|/Gb, for some selected BCPs of product-1 and product-2 and their corresponded transition states, respectively. The QTAIM molecular graphs of product-1, product-2 and their corresponded transition states have been displayed in Figs. 5 and 6, respectively.

It should be mentioned that the aforementioned properties of

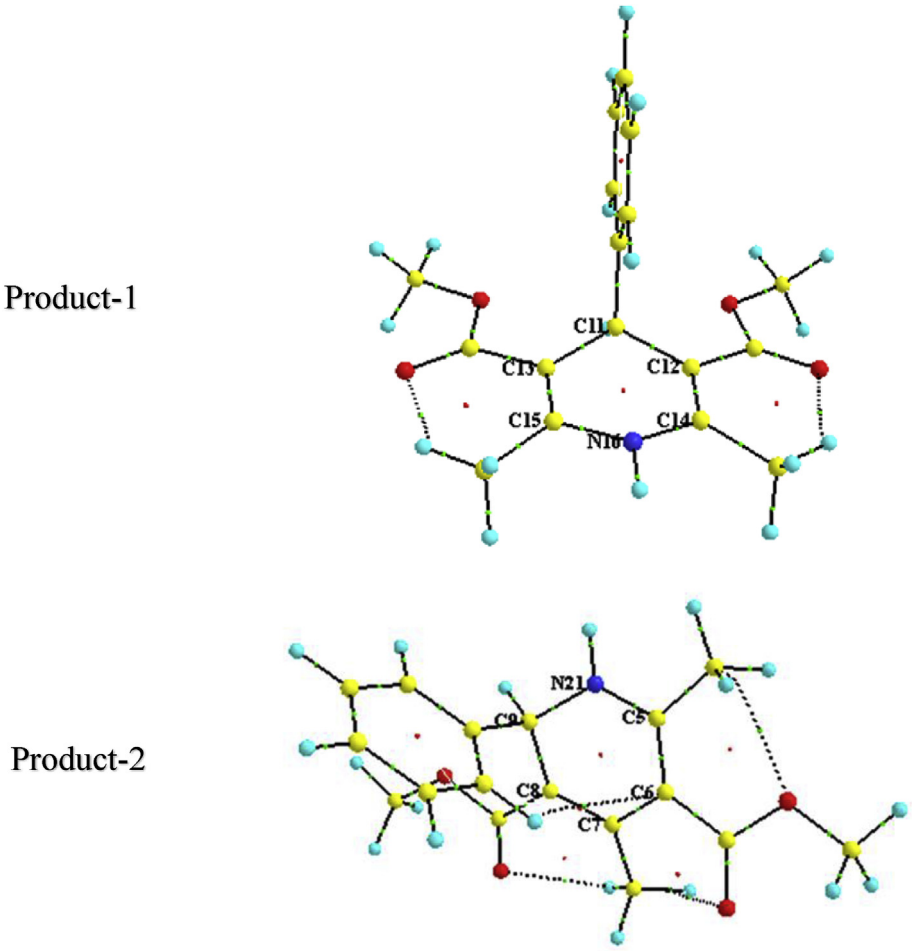

Fig. 5. QTAIM molecular graphs of product-1 and product-2 calculated at M08-HX/6-311 + G** level of theory.

electron density at BCPs can be regarded as the regions of concentration and depletion of electron charge density and a basis for classifying the interatomic interactions [60,61].

The comparative investigation of the reported results in Tables 7 and 8 clearly show the following facts: (i) the negative values of $\nabla 2\rho$ and also H(r) at all selected BCPs determine the presence of covalent bond critical points and consequently charge concentration in the bonded region, (ii) comparison between the calculated electron density properties and indicators on C11—C13 and N16—C14 as newly formed covalent bonds in product-1 with the corresponded C6—C7 and N21—C9 bonds in product-2 shows that C11—C13 in product-1 is more strongly than C6—C7 in product-2, while there is an inverse trend in the bond strength of N16—C14 in product-1 compared with N21—C9 in product-2. In the other point, it can be claimed that product-2 is more stable electronically based on the formation of more ring critical points (RCP) around the pyridine ring, (iii) comparative assessment on the near value of electron density for C6—C8 and C6—C9 in TS-1 and TS-2, respectively, reveals no preference from the electronic viewpoint while in QTAIM molecular graph of TS-1, it has been displayed more RCPs around C6—C8 that leads to the more electronic stability of TS-1. This feature can be regarded as the main electronic origin for the priority of reaction path-1 in comparison with reaction path-2.

5. Conclusion

In summary, in this paper, we reported an effective, versatile and facile strategy for the synthesis of polyhydroquinoline derivatives *via* Hantzsch MCR employing BWA as a green, reusable and homogeneous catalyst in refluxing EtOH. This strategy not only demonstrates significant improvements in the rate of reaction and provide higher yields, but also circumvents the utilization of hazardous catalysts or solvents. The gifted points for the presented strategy are competence, and generality, obtaining high yields in relatively short reaction time, clean reaction profile, simplicity of product isolation, uncomplicatedness, latent for recycling of the catalyst. In the other hand, we investigated the energetics of two different reaction pathways that lead to generate the different products, 1,4-DHPs and 2-arylpyridines, using quantum chemistry methods. In this line, thermochemical and electronic features of two reaction pathways and their corresponded transition states were analyzed *via* DFT and QTAIM approaches. The calculated thermochemical and electronic results clearly demonstrated the mechanistical priority in the synthesis of 1,4-DHPs than 2-arylpyridines. Notably, the purpose of this work, is presenting a green, homogenous catalyst with potential usage for improving organic reactions and synthesis of 1,4-DHPs is just particular as a model organic transformation.

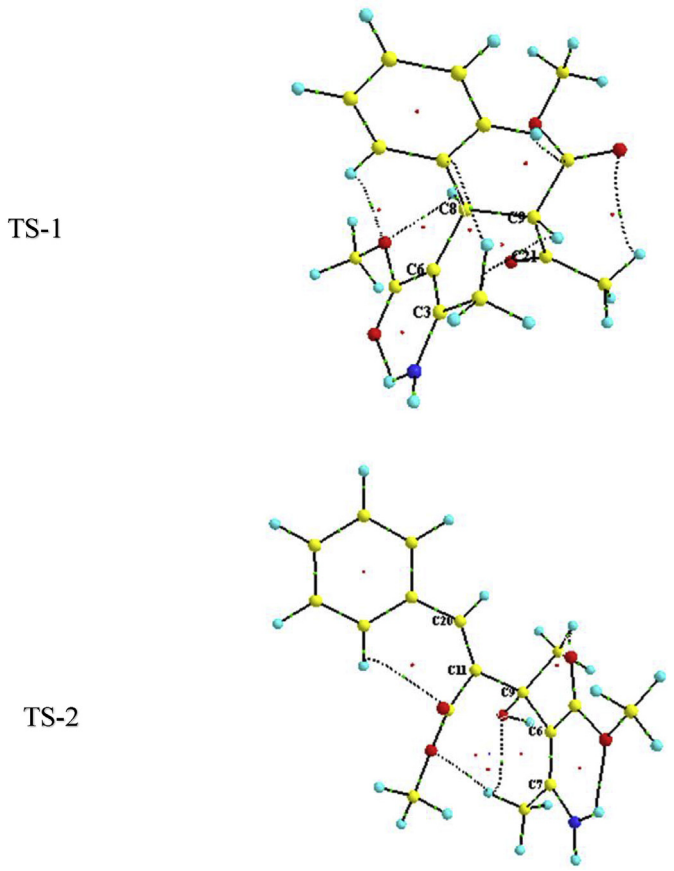

Fig. 6. QTAIM molecular graphs of TS-1 and TS-2 calculated at M08-HX/6-311 + G** level of theory.

Acknowledgements

The authors are thankful from Alzahra Research Council for the partial financial support. MMH is also thankful to Iranian National Science Foundation (INSF) for partial financial support. MM is thankful to research council of Ferdowsi University of Mashhad, Mashhad, Iran.

Appendix A. Supplementary data

Supplementary data to this article can be found online at https://doi.org/10.1016/j.molstruc.2019.127011.

References

[1] B.B. Toure, D.G. Hall, Natural product synthesis using multicomponent reaction strategies, Chem. Rev. 109 (2009) 4439–4486.
[2] A. Shaabani, A. Sarvary, S. Ghasemi, A.H. Rezayan, R. Ghadari, S.W. Ng, An environmentally benign approach for the synthesis of bifunctional sulfonamide-amide compounds viaisocyanide-based multicomponent reactions, Green Chem. 13 (2011) 582–585.
[3] A. Zhu, R. Liu, Ch Dua, L. Lia, Betainium-based ionic liquids catalyzed multicomponent Hantzsch reactions for the efficient synthesis of acridinediones, RSC Adv. 7 (2017) 6679–6684.
[4] (a) D.J. Triggle, 1,4-dihydropyridine calcium channel ligands: selectivity of action. The roles of pharmacokinetics, state-dependent interactions, channel isoforms, and other factors, Drug Dev. Res. 58 (2003) 5–17;
(b) J.-C. Liang, J.-L. Yeh, C.-S. Wang, S.-F. Liou, C.-H. Tsai, I.-J. Chen, The new generation dihydropyridine type calcium blockers, bearing 4-phenyl oxypropanolamine, display α-/β-Adrenoceptor antagonist and long-Acting antihypertensive activities, Bioorg. Med. Chem. 10 (2002) 719–730;
(c) N. Edraki, A.R. Mehdipour, M. Khoshneviszadeh, R. Miri, Dihydropyridines: evaluation of their current and future pharmacological applications, Drug Discov. Today 14 (2009) 1058–1066;
(d) M. Mirela Filipan-Litvíc, M. Litvíc, I. Cepanec, V. Vinkovíc, Hantzsch Synthesis of 2,6-Dimethyl-3,5-dimethoxycarbonyl-4-(o-methoxyphenyl)-1,4-dihydropyridine; a Novel cyclisation leading to an unusual formation of 1-amino-2-methoxycarbonyl-3,5-bis(o-methoxyphenyl)-4-oxa-cyclohexan-1-ene, Molecules 12 (2007) 2546–2558.
[5] M.G. Dekamin, S. khanizadeh, Z. Latifidoost, H. Daemi, Z. Karimi, M. Barikani, Alginic acid: a highly efficient renewable and heterogeneous biopolymeric catalyst for one-pot synthesis of the Hantzsch 1,4-dihydropyridines, RSC Adv. 4 (2014) 56658–56664.
[6] (a) T. Godfraid, R. Miller, M. Wibo, Calcium antagonism and calcium entry blockade, Pharmacol. Rev. 38 (1986) 321–416;
(b) A. Sausins, G. Duburs, Synthesis of 1, 4-dihydropyridines by cyclocondensation reactions, Heterocycles 27 (1988) 269–289;
(c) P.P. Mager, R.A. Coburn, A.J. Solo, D.J. Triggle, H. Rothe, QSAR, diagnostic statistics and molecular modelling of 1, 4-dihydropyridine calcium antagonists: a difficult road ahead, Drug Des. Discov. 8 (1992) 273–289;
(d) R. Mannhold, B. Jablonka, W. Voigdt, K. Schoenafinger, K. Schravan, Calcium-and calmodulin-antagonism of elnadipine derivatives: comparative SAR, Eur. J. Med. Chem. 27 (1992) 229–235.
[7] B. Love, K.M. Sander, The Hantzsch reaction. I. Oxidative dealkylation of certain dihydropyridines, J. Org. Chem. 30 (1965) 1914–1916 (Cover letter).
[8] (a) A. Hantzsch, Synthese von thiazolen und oxazolen, Ber. Dtsch. Chem. Ges. 21 (1888) 942–946;
(b) A. Hantzsch, Neue bildungsweise yon pyrrolderivaten, Ber. Dtsch. Chem. Ges. 23 (1890), 1747-1476;
(c) R.H. Wiley, D.C. England, L.C. Behr, in: Organic Reactions vol. 1, Wiley, Toronto, 1951, p. 367, 6;
(d) A. Dondoni, A. Massi, E. Minghini, V. Bertolasi, Multicomponent Hantzsch cyclocondensation as a route to highly functionalized 2- and 4-dihydropyridylalanines, 2- and 4-pyridylalanines, and their *N*-oxides: preparation *via* a polymer-assisted solution-phase approach, Tetrahedron 60 (2004) 2311–2326.
[9] Sh Ko, Ch-F. Yao, Ceric Ammonium Nitrate (CAN) catalyzes the one-pot synthesis of polyhydroquinoline *via* the Hantzsch reaction, Tetrahedron 62 (2006) 7293–7299.
[10] A. Hardwick, P.G. Dickens, R.C.T. Slade, Investigation of H^+ motion in the 21-hydrates of 12-tungstophosphoric and 12-molybdophosphoric acids by ac conductivity and pulsed 1H NMR measurements, Solid State Ion. 13 (1984) 345–350.
[11] K.D. Kreuer, M. Hampele, K. Dolde, A. Rabenau, Proton transport in some heteropolyacidhydrates a single crystal PFG-NMR and conductivity study, Solid State Ion. 28–30 (1988) 589–593.
[12] R.C.T. Slade, H.A. Pressman, E. Skou, Ac and dc conductivity studies of pelletised 12-tungstophosphoric acid and 12-tungstosilicic acid hexahydrates, Solid State Ion. 38 (1990) 207–211.
[13] R.C.T. Slade, J. Barker, H.A. Pressman, Studies of protonic self-diffusion and conductivity in 12-tungstophosphoric acid hydrates by pulsed field gradient ^{1}H NMR and ac conductivity, Solid State Ion. 28–30 (1988) 594–600.
[14] U.B. Miöc, M.R. Todorovíc, M. Davidovíc, P. Colomban, I. Holclajtner-Antunovíc, Heteropoly compounds-From proton conductors to biomedical agents, Solid State Ion. 176 (2005) 3005–3017.
[15] M. Sadakane, E. Steckhan, Electrochemical properties of polyoxometalates as electrocatalysts, Chem. Rev. 98 (1998) 219–238.
[16] D.E. Katsoulis, A survey of applications of polyoxometalates, Chem. Rev. 98 (1998) 359–388.
[17] R.S. Drago, J.A. Dias, T.O. Maier, An acidity scale for Brönsted acids including $H_3PW_{12}O_{40}$, J. Am. Chem. Soc. 119 (1997) 7702–7710.
[18] F. Lefebvre, F.X. Liu-Cai, A. Auroux, Microcalorimetric study of the acidity of tungstic heteropolyanions, J. Mater. Chem. 4 (1994) 125–131.
[19] M.M. Heravi, F.K. Behbahani, F.F. Bamoharram, $H_{14}[NaP_5W_{30}O_{110}]$: a heteropoly acid catalyzed acetylation of alcohols and phenols in acetic anhydride, J. Mol. Catal. A Chem. 253 (2006) 16–19.
[20] M.M. Heravi, Kh Bakhtiari, F.F. Bamoharram, An efficient and chemoselective synthesis of acylals from aromatic aldehydes and their regeneration, catalyzed by 12-molybdophosphoric acid, Catal. Commun. 7 (2006) 499–501.
[21] M.M. Heravi, Kh Bakhtiari, T. Benmorad, F.F. Bamoharram, H.A. Oskooie, M.H. Tehrani, Nitration of aromatic compounds catalyzed by divanadium-substituted molybdophosphoric acid, $H_5[PMo_{10}V_2O_{40}]$, Monatshefte Chem. 138 (2007) 449–452.
[23] M.M. Heravi, M. Mirzaei, S.Y. Shirazi Beheshtiha, V. Zadsirjan, F. Mashayekh Ameli, M. Bazargan, $H_5BW_{12}O_{40}$ as a green and efficient homogeneous but recyclable catalyst in the synthesis of 4H-Pyrans via multicomponent reaction, Appl. Organomet. Chem. 32 (2018) e4479.
[24] M.M. Heravi, Z. Faghihi, Applications of heteropoly acids in multi-component reactions, J. Iran. Chem. Soc. 11 (2014) 209–224.
[25] M.M. Heravi, M. Vazin Fard, Z. Faghihi, Heteropoly acids-catalyzed organic reactions in water: doubly green reactions, Green Chem. 6 (2013) 282–300.
[26] T. Hosseinnejad, M. Omrani-Pachin, M.M. Heravi, Joint computational and experimental investigations on the synthesis and properties of Hantzsch-type compounds: an Overview, Curr. Org. Chem. 23 (2019) 1–18.
[27] M. Malmir, M.M. Heravi, S. Sadjadi, T. Hosseinnejad, Ultrasonic and bio-assisted synthesis of Ag@HNTs-T as a novel heterogeneous catalyst for the green synthesis of propargylamines: a combination of experimental and computational study, Appl. Organomet. Chem. 32 (2018), e4291.

[28] T. Baie Lashaki, H.A. Oskooie, T. Hosseinnejad, M.M. Heravi, CuI nanoparticles on modified poly (styrene-co-maleic anhydride) as an effective catalyst in regioselective synthesis of 1, 2, 3-triazoles via click reaction: a joint experimental and computational study, J. Coord. Chem. 70 (2017) 1815–1834.
[29] V. Zadsirjan, M.M. Heravi, M. Tajbakhsh, H.A. Oskooie, M. Shiri, T. Hosseinnejad, Hydroarylation of cinnamic acid with phenols catalyzed by acidic ionic liquid [H-NMP]HSO_4: computational assessment on substituent effect, Res. Chem. Intermed. 42 (2016) 6407–6422.
[30] M.M. Heravi, T. Hosseinnejad, N. Nazari, Computational investigations on structural and electronic properties of CuI nanoparticles immobilized on modified poly(styrene-co-maleic anhydride) leading to an unexpected but efficient catalyzed synthesis of 1,4-dihydropyridine via Hantzsch pyridine synthesis, Can. J. Chem. 92 (2017) 530–536.
[31] T. Hosseinnejad, S. Mahdavian, Quantum chemistry study on regioselectivity in ruthenium catalyzed synthesis of 1,5-disubstituted 1,2,3-triazoles, Comput. Theor. Chem. 1143 (2018) 29–35.
[32] T. Hosseinnejad, M. Dinyari, Computational study on stereoselective synthesis of substituted 1H-tetrazoles via a click reaction: DFT and QTAIM approaches, Comput. Theor. Chem. 1071 (2015) 53–60.
[33] T. Hosseinnejad, M.M. Heravi, R. Firouzi, Regioselectivity in Sonogashira synthesis of 6-(4-nitrobenzyl)-2-phenylthiazolo[3,2-*b*]1,2,4-triazole: a quantum chemistry study, J. Mol. Model. 19 (2013) 951–961.
[34] H. Gao, A. Virya, K. Lian, Proton conducting $H_5BW_{12}O_{40}$ electrolyte for solid supercapacitors, J. Mater. Chem. A. 3 (2015) 21511–21517.
[35] T. Demirci, B. Çelik, Y. Yıldız, S. Eriş, M. Arslan, F. Sen, B. Kilbas, One-pot synthesis of Hantzsch dihydropyridines using a highly efficient and stable PdRuNi@GO catalyst, RSC Adv. 6 (2016) 76948–76956.
[36] M. Hong, Ch Cai, W.-B. Yi, Hafnium (IV) bis(perfluorooctanesulfonyl)imide complex catalyzed synthesis of polyhydroquinoline derivatives via unsymmetrical Hantzsch reaction in fluorous medium, J. Fluorine Chem. 131 (2010) 111–114.
[37] Q. Zhang, X.-M. Ma, H.-X. Wei, X. Zhaoa, J. Luoc, Covalently anchored tertiary amine functionalized ionic liquid on silica coated nano-Fe3O4 as a novel, efficient and magnetically recoverable catalyst for the unsymmetrical Hantzsch reaction and Knoevenagel condensation, RSC Adv. 7 (2017) 53861–53870.
[38] H. Niaz, H. Kashtoh, J.A.J. Khan, A. Khan, A.-T. Wahab, M. Tanveer Alam, Kh Mohammed Khan, Sh Perveen, M. Iqbal Choudhary, Synthesis of diethyl 4-substituted-2,6-dimethyl-1,4-dihydropyridine-3,5-dicarboxylates as a new series of inhibitors against yeast α-glucosidase, Eur. J. Med. Chem. 95 (2015) 199–209.
[39] S.M. Vahdat, F. Chekin, M. Hatami, M. Khavarpour, S. Bagheri, Z. Roshan-kouhi, Synthesis of polyhydroquinoline derivatives via a four-component Hantzsch condensation catalyzed by tin dioxide nanoparticles, Chin. J. Chem. 34 (2013) 758–763.
[40] A. Debache, W. Ghalem, R. Boulcina, A. Belfaitah, S. Rhouati, B. Carboni, An efficient one-step synthesis of 1,4-dihydropyridines via a triphenylphosphine-catalyzed three-component Hantzsch reaction under mild conditions, Tetrahedron Lett. 50 (2009) 5248–5250.
[41] M.M. Heravi, V. Zadsirjan, B. Fattahi, N. Nazari, Applications of dimedone in the synthesis of heterocycles: an update, Curr. Org. Chem. 20 (2016) 1676–1735.
[42] U.C. Reddy, S. Bondalapati, A.K. Saikia, Stereoselective One-Pot, three-component synthesis of 4-aryltetrahydropyran *via* Prins-Friedel-Crafts reaction, J. Org. Chem. 74 (2009) 2605–2608.
[43] U.C. Reddy, A.K. Saikia, One-pot, three-component synthesis of 4-aryl-5,6-dihydropyran *via* prins-friedel-crafts reaction, Synlett 7 (2010) 1027–1032.
[44] U.C. Reddy, B. Rama Raju, E.K. Pramod Kumar, A.K. Saikia, Stereoselective one-pot, three-component synthesis of 4-amidotetrahydropyran, J. Org. Chem. 73 (73) (2008) 1628–1630.
[45] B.B.F. Mirjalili, A. Bamoniri, L. Asadollah Salmanpoor, $TiCl_2$/Nano-γ-Al_2O_3 as a novel lewis acid catalyst for promotion of one-pot synthesis of 1,4-dihydropyridines, J. Nanostruct. 8 (2018) 276–287.
[46] E. Mosaddegh, A. Hassankhani, One-pot synthesis of polyhydropyridine derivatives *via* Hantzsch four component condensation in water medium: use of a recyclable Lewis acid [$Ce(SO_4)_2.4H_2O$] catalyst, Bull. Chem. Soc. Ethiop. 26 (2012) 461–465.
[47] M. Maheswari, V. Vasudevan Srinivasan, A. Ramanathan, M.P. Pachamuthu, R. Rajalakshmi, G. Imran, Preparation and characterization of mesostructured Zr-SBA-16: efficient Lewis acidic catalyst for Hantzsch reaction, J. Porous Mater. 22 (2015) 705–711.
[48] M.M. Heravi, M. Saeedi, N. Karimi, M. Zakeri, Y.S. Beheshtih, A. Davoodnia, Brønsted acid ionic liquid [$(CH_2)_4SO_3HMIM$][HSO_4] as novel catalyst for one-pot synthesis of Hantzsch polyhydroquinoline derivatives, Synth. Commun. 40 (2010) 523–529.
[49] N. Devarajana, P. Suresh, MIL-101-SO_3H metal-organic framework as a Brønsted acid catalyst in Hantzsch reaction: an efficient and sustainable methodology for one-pot synthesis of 1,4-dihydropyridine, New J. Chem. 43 (2019) 6806–6814.
[50] X. Liu, B. Liu, Hantzsch reaction starting directly from alcohols through a tandem oxidation process, J. Chem. 2017 (2017) 1–5.
[51] A. Davoodnia, M. Khashi, N. Tavakoli-hoseini, Tetrabutylammonium hexatungstate [TBA]$_2$[W_6O_{19}]: novel and reusable heterogeneous catalyst for rapid solvent-free synthesis of polyhydroquinoline via unsymmetrical Hantzsch reaction, Chin. J. Catal. 34 (2013) 1173–1178.
[52] D. Elhamifar, H. Khanmohammadia, D. Elhamifar, Nickel containing ionic liquid based ordered nanoporous organosilica: a powerful and recoverable catalyst for synthesis of polyhydroquinolines, RSC Adv. 7 (2017) 54789–54796.
[53] T. Demirci, B. Çelik, Y. Yıldız, S. Eris, M. Arslan, F. Sen, B. Kilbas, One-pot synthesis of Hantzsch dihydropyridines using a highly efficient and stable PdRuNi@GO catalyst, RSC Adv. 6 (2016) 76948–76956.
[54] G.B. Dharma Rao, S. Nagakalyan, G.K. Prasad, Solvent-free synthesis of polyhydroquinoline derivatives employing mesoporous vanadium ion doped titania nanoparticles as a robust heterogeneous catalyst via the Hantzsch reaction, RSC Adv. 7 (2017) 3611–3616.
[55] L.-M. Wang, J. Sheng, L. Zhang, J.-W. Han, Zh-Y. Fan, H. Tiana, Ch-T. Qian, Facile Yb(OTf)$_3$ promoted one-pot synthesis of polyhydroquinoline derivatives through Hantzsch reaction, Tetrahedron 61 (2005) 1539–1543.
[56] L. Shen, S. Cao, J. Wu, J. Zhang, H. Li, N. Liu, X. Qian, A revisit to the Hantzsch reaction: unexpected products beyond 1,4-dihydropyridines, Green Chem. 11 (2009) 1414–1420.
[57] W. Schmidt, M.K. Baldridge, K.A. Boatz, J.T. Elbert, S.S. Gordon, M.H. Jensen, J. Koseki, S. Matsunaga, N.A. Nguyen, K.J. Su, S.L. Windus, T. Dupuis, M.A. Montgomery, General atomic and molecular electronic structure system, J. Comput. Chem. 14 (1993) 1347–1363.
[58] Y. Zhao, D.G. Truhlar, Exploring the limit of accuracy of the global hybrid meta density functional for main-group thermochemistry, kinetics, and noncovalent interactions, J. Chem. Theory Comput. 4 (2008) 1849–1868.
[59] R.F.W. Bader, AIM2000 Program, Mc Master University, Hamilton, 2000, version 2.0.
[60] E. Espinosa, I. Alkorta, J. Elguero, E. Molins, From weak to strong interactions: a comprehensive analysis of the topological and energetic properties of the electron density distribution involving X–H···F–Y systems, J. Chem. Phys. 117 (2002) 5529.
[61] R.G. Bone, R. F Bader, Identifying and analyzing intermolecular bonding interactions in van der Waals molecules, J. Chem. Phys. 100 (1996) 10892–10911.